analytical chemistry

pubs.acs.org/ac Article

Monte Carlo Simulation Aided Quantitative Laboratory X-ray Fluorescence Analysis and Its Application in Provenancing Studies for Geo-Archeological Samples

Brecht Laforce,* Géraldine Fiers, Hans Vandendriessche, Philippe Crombé, Veerle Cnudde, and Laszlo Vincze

Cite This: *Anal. Chem.* 2021, 93, 3898−3904 Read Online

ACCESS | Metrics & More | Article Recommendations

ABSTRACT: A laboratory-based X-ray fluorescence (XRF) methodology is presented for standardless quantified analysis based on a monochromatic X-ray spectrometer coupled to Monte Carlo aided quantification. This procedure will be valuable for many scientific fields (e.g. archaeology, geology, etc.) where the unique nature of the investigated samples calls for the application of non-destructive techniques. To illustrate the value of the methodology, a case study is presented where flint artefacts from the Scheldt basin are analyzed in an attempt to provenance them. So far, little geochemical research has been done in this area. Our results contribute to the creation of a database that will help assign lithic artefacts to specific geological outcrops and will aid further research in this field.

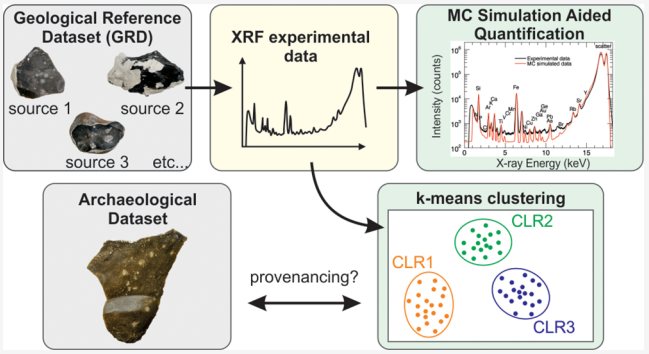

INTRODUCTION

Monochromatic X-ray fluorescence (XRF) analysis, coupled with state-of-the-art quantification methodologies, has long proven its great value to many scientific fields through the vast number of experiments performed at various synchrotron beamlines.[1−6] Recent developments in laboratory XRF instrumentation and further progress of quantification methodologies have made these techniques a viable option in the lab, showing promising results.[7−9] The implementation of these developments at the in-house developed, monochromatic microXRF instrument at our Ghent University laboratory allows for relatively quick and easy, standardless quantification of XRF mappings on numerous types of materials.

In archaeological and cultural heritage studies, provenancing of materials is of major interest when studying artefacts. Chemical fingerprinting based on trace element composition of the samples in question is crucial in this aspect, as well as the availability of an adequate reference database. At Ghent University, we aim at developing a standardized procedure to perform this type of experiments using monochromatic laboratory-based XRF with standardless quantification based on Monte Carlo (MC) simulation aided routines.

For archaeologists studying prehistoric societies, lithic provenancing studies are of utmost importance to gain a better understanding of hunter-gatherer territories, mobility, land-use practices, and techno-economic behavior. Such provenancing efforts often combine traditional macroscopic approaches with the analysis of thin-sections, micropalaeontological, and geochemical methods. Although early attempts to source obsidian and flint outcrops using geochemical methods date to the 1960 and 1970's,[10,11] the application of geochemical methods to discriminate between different flint varieties has only become widely used in the last two decades, for example by making use of XRF,[12−16] LA-ICP−MS,[14,17−22] and Raman and infrared spectroscopy.[15,23−25]

In our study area, Northwest Belgium, primary flint outcrops are absent. The only flint nodules locally available are included in residual, Early Pleistocene gravel beds of the river Scheldt or are washed up onto the North Sea shores. They are qualitatively inferior (small dimensions and incipient fissures) and hence not always suited for stone toolmaking. Better quality raw materials were therefore frequently imported from the adjacent regions to the south with primary Cretaceous flint outcrops:[26] the Northeast of France and the Tournai area, the Mons Basin, and the Hesbaye/Limburg area.

Received: October 30, 2020
Accepted: February 9, 2021
Published: February 18, 2021

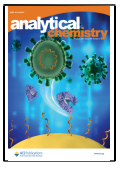

https://dx.doi.org/10.1021/acs.analchem.0c04583
Anal. Chem. 2021, 93, 3898−3904

Table 1. Overview of Geological Flint Samples Used for Bulk and Micro XRF Analyses

flint type	area	geological stage of host rock	bulk XRF	μXRF
Spiennes	Mons basin (BE)	Campanian	13	3
Spiennes, light grey variety	Mons basin (BE)	Campanian	11	2
Obourg	Mons basin (BE)	Campanian	10	1
Haubourdin	Northeast of France (FR)	Coniacian	11	2
Bouvines	Northeast of France/Tournaisis (FR)	middle/upper Turonian	11	3
Esplechin	Tournaisis (BE)	upper Turonian	10	2
Froyennes	Tournaisis (BE)	middle/upper Turonian	6	1
Ère	Tournaisis (BE)	middle/upper Turonian	6	1
Vlissingen	North Sea shores (NL)	unknown	14	1

Reliably assigning lithic artefacts to one of these major outcrop areas can, however, be problematic or even impossible, based on macroscopic characteristics alone.[27−29] Additional in-depth characterization methods are thus required to distinguish between different flint types.

Although only limited research has been done on this topic so far in Belgium, recent research on Mons basin flints[14,23] confirmed the effectiveness of geochemical analysis to achieve this. In addition, in a previous paper,[30] we reported the results of XRF-analysis performed on geological samples of six different flint types from Northeast France, the Mons basin, and the beaches of the Scheldt estuary. Following the promising results of this study, a decision was made to expand the analysis by including archaeological samples to further assess the potential of XRF to discriminate between the flint types exploited in NW Belgium.

EXPERIMENTAL SECTION

Geological Flint Samples. The geological flint samples were procured from various locations in northwestern Belgium and neighboring areas in France and the Netherlands during different field excursions[30] (Table 1). These locations are considered to represent possible supply sources for the prehistoric societies who lived in the Scheldt river basin. In the Mons Basin, flint samples were collected from Campanian chalk layers in the Omya Benelux Ltd. quarry near Harmignies (Spiennes flint) and in the Holcim Ltd. quarry near Obourg (Obourg flint). In the northeast of France, Haubourdin flint was sampled from Coniacian chalk layers in the Recynor quarry. Furthermore, flint collected as surface finds (from sub-autochtonous and secondary context) of middle to upper Turonian age was retrieved from the localities Bouvines, Esplechin, Froyennes, and Ère near Tournai. Finally, the locally used pebble flint was taken into consideration, and flint samples were collected from the shores of the North Sea near Vlissingen (secondary context). Based on the previous bulk XRF results,[30] 16 representative samples were selected to perform μXRF measurements (Table 1).

The geological reference dataset consisted of 16 samples. One to three samples were selected for each reference site. These samples were cut and polished, providing a nice smooth surface for XRF analysis. On each sample, a 3 × 2 point mapping was performed with 2 mm distance between the individual points. This way, an average composition of a relatively large area of flint material was measured, and the probability of heterogeneities in the samples to disturb the results was minimized. The XRF spectra were collected during 3000 s live time, with the tube operating at 40 kV and 0.8 mA.

Archaeological Flint Samples. 18 flint artefacts from eight archaeological sites in the Scheldt basin were selected for this test-case. These sites cover a large geographical area (from the French border to the estuary near Antwerp) and a relatively long timespan, that is, from the Final Paleolithic to the Middle Neolithic period (ca. 12,500−3600 cal. BC).

Based on their macroscopic features, ten artefacts are expected to originate from the middle to upper Turonian of the Tournai-Lille area. Two artefacts are further identified as possible Spiennes flints and three others as either Obourg or Haubourdin type flints. Finally, two artefacts are made of pebble flints that were possibly collected from the North Sea beaches, and a last artefact, from the site of Oeudeghien, is interpreted as a Turonian flint from the Mons basin. Only this last artefact has no potential counterpart among the geological samples.

XRF Instrument. The XRF experiments were performed on an in-house developed spectrometer, the micro-XRF as described by Garrevoet and colleagues.[9,31] Prior to the work described in this paper, the setup was refitted with a new X-ray tube (XOS, East Greenbush NY, US). This new tube is an upgraded version of the Mo tube used previously, employing DCC optics to generate a monochromatic micro-beam (at 17.48 keV, i.e. Mo Kα) with a spot size of approximately 220 μm full width half maximum.

A further optimization of the system aimed at maximizing the reproducibility of sample positioning. A digital microscope (Dino-Lite, Taiwan) and a laser triangulation system (Micro-Epsilon, Ortenburg, Germany) were placed in a fixed configuration in the spectrometer, allowing for a robust and multi-modal check of the sample position. The laser triangulation system has a precision along the X-ray beam of 4 μm, which is much smaller than the depth of focus of the X-ray tube (∼250 μm) and thus allows for adequate and repeatable positioning of the sample relative to the frame of reference of the spectrometer. Next, the digital microscope is positioned such that the image of the sample is only sharp when near the plane of focus. Finally, since the laser spot can be seen on the sample, this allows for a further visual check of the focusing and is an aid in determining the position of the X-ray beam.

The upgraded instrument allows monochromatic XRF experiments with limits of detection below 10 ppm for a wide range of elements (Figure 1) using a 100 μm thick MPI DING KL2-G as the reference material.[32]

Quantification Procedure. The XRF spectra were analyzed using the AXIL algorithm,[33] a linear least square fitting procedure, yielding the intensity for each detectable element in the samples. To establish a fast quantification method for the described spectrometer, a MC simulation aided quantification method was used.[8,34]

https://dx.doi.org/10.1021/acs.analchem.0c04583
Anal. Chem. 2021, 93, 3898−3904

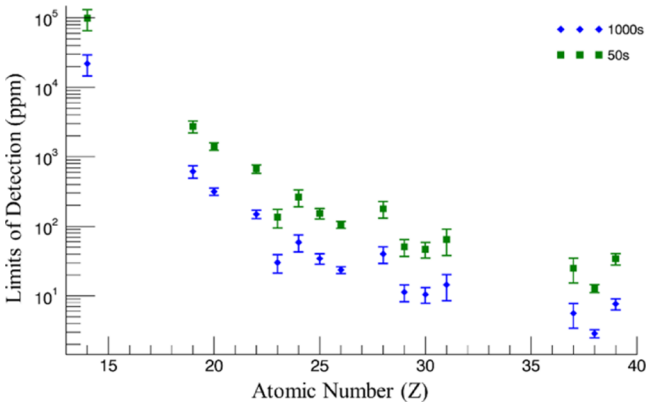

Figure 1. Limits of detection for the upgraded microXRF instrument, scan on MPI DING KL2-G; 40 kV, 0.8 mA, 1000 s live time and extrapolation to 50 s.

The first step involved building the virtual version of the instrument using scans on three different reference materials (NIST SRM 2709a, NIST SRM 1577c, and MPI DING ATHO-G).[32] These materials were chosen since they have very different matrices, being a soil sample, organic material, and basalt glass, respectively. Using the reference composition of these materials, the spectrometer parameters (e.g. angle between source and detector, detector-sample distance, and sample-source distance) were optimized until the simulated and experimental spectra coincided.

Once the simulation was optimized, experiments at different tube settings were employed to check the validity of the assumptions made during the construction of the model. Finally, a set of 18 reference materials was used to validate the model. These references included soil samples, glasses, metal alloys, organic materials, and thin film reference materials in order to maximize the variety of sample matrices. The results of these simulations were then used to assess the quality of the quantification procedure. Each reference material was treated as an unknown sample and quantified through the iterative quantification procedure as described by Schoonjans et al.[8] For all detectable elements, the difference between the concentration obtained via this procedure and the referenced value was used as a measure of the experimental error. The deviation between reference value and the concentration obtained through the MC aided quantification method varied between 3.5% for Zr (based on 6 reference materials) to 17% for Ti (based on 11 reference materials) with 2/3 of the elements deviating less than 10% from the certified values based on multiple reference materials (Table 3).

The optimized MC simulation protocol allows for standardless quantification of any type of material using the micro-XRF spectrometer. This makes quantitative XRF experiments considerably more straightforward and leads to a fast and elegant laboratory-based analysis tool.

Provenancing of Flint Materials: *k*-Means Routine. To link the archaeological flint materials to specific locations, a procedure based on *k*-means clustering[35−37] was used. In a first step, the geological reference samples were scanned. On each sample, 6 different point measurements of 3000 s live time were recorded (minimal interspacing of 1 mm), with the tube operating at 40 kV and 0.8 mA. The archaeological artefacts were scanned using the same procedure as the reference samples. The XRF spectra were analyzed using AXIL[33] to retrieve the intensities of all detectable elements. In-house developed software[36] was then used to divide the reference scans in 10 different clusters (one for each location of origin) employing a *k*-means algorithm. Clustering was performed on the non-quantified data to minimize prior data treatment which could interfere with the clustering outcome.

The *k*-means algorithm generates a center of mass for each of its clusters, which can be considered the reference value for a specific cluster. To provenance the archeological materials, the Euclidian distance between each XRF point measurement and the mean cluster values are calculated, as would be the case in the regular *k*-means clustering algorithm. However, the procedure deviates from this algorithm in the further steps taken once these Euclidian distances are known, since the possibility exists that one or more of the artefacts came from a location not included in the reference set.

Based on the data set of the geological reference materials, for each element in each cluster an expectancy interval is constructed. This interval lies symmetrically around the cluster mean value and is defined as the maximal difference between a point value and the cluster mean within the reference dataset, increased by two times the standard deviation.

Before a point in the archeological dataset is allocated to a cluster, both the Euclidian distances need to be minimal and

Table 2. Overview of Selection of Archaeological Artefacts Measured with μXRF

short ID	site location	raw material type
BA1	Bazel Sluis	Scheldt flint
BA2	Bazel Sluis	Obourg
DD1	Doel Deurganckdok	Scheldt flint
DD2	Doel Deurganckdok	Scheldt flint
DD3	Doel Deurganckdok	North Sea basin flint
DD4	Doel Deurganckdok	North Sea basin flint
DD5	Doel Deurganckdok	Spiennes
DD6	Doel Deurganckdok	Grey fine-grained
KH1	Kerkhove Stuw	Scheldt flint
KH2	Kerkhove Stuw	Scheldt flint (chalky variety)
KH3	Kerkhove Stuw	Grey fine-grained, internal speckles
KK1	Kruishoutem Kerkakkers	Scheldt flint
OD1	Oudenaarde Donk Neo 1	Scheldt flint
OD2	Oudenaarde Donk 2003	Scheldt flint
OE1	Oeudeghien	Turonian Mons basin
RU1	Ruien Rosalinde	Scheldt flint
VA1	Verrebroek Aven Ackers	Scheldt flint
VA2	Verrebroek Aven Ackers	Spiennes

Table 3. Average Difference between MC Aided Quantification and Certified Reference Value for the Elements of Relevance for This Study (av. diff.) and the Number of Reference Materials This Value Is Based on (*n*)[a]

element	av. diff. (%)	*n*	element	av. diff. (%)	*n*
Si	10.2	12	Ni	10.6	13
P	6.2	2	Cu	7.2	15
K	12.2	12	Zn	4.5	15
Ca	11.2	15	As	8.5	8
Ti	16.7	11	Rb	4.3	11
V	8.9	12	Sr	7.7	13
Cr	10.2	11	Y	9.2	8
Mn	8.7	14	Zr	3.5	6
Fe	9.3	16	Pb	6.7	8

[a]Of the 18 elements, 6 scored worse than 10%.

https://dx.doi.org/10.1021/acs.analchem.0c04583
Anal. Chem. 2021, 93, 3898−3904

no more than two elements can be outside the expectancy interval.

RESULTS

Geological Reference Dataset. The *k*-means clustering on the reference dataset had multiple objectives: (a) proving the feasibility of subdividing a set of flint samples in coherent clusters using the *k*-means algorithm, (b) studying the similarities between different geological references sites, and (c) creating the reference framework on which the provenancing could later on be based.

Six clusters proved to contain the bulk of the data points: cluster 1 grouping all Haubourdin samples with the sample from Vlissingen and the Obourg sample, cluster 2 containing the light grey Spiennes samples, cluster 3 with the bulk of the Spiennes samples, cluster 4 with the samples from Ère and one of the Esplechin flints, cluster 5 with the second Esplechin, and cluster 9 with the Bouvines and Froyennes materials. The other clusters contained few points and were most likely linked to inclusions in the flint materials. Two of these, clusters 6 and 7, contained points of the Spiennes samples, while cluster 8 belonged to light grey Spiennes materials and cluster 10 contained a single point of the Esplechin samples. Table 4 gives an overview of the cluster compositions.

Table 4. Distribution of the Geological Reference Samples over the Clusters, with the Number of Points Attributed to Each Cluster

CLR1	24 points	Haubourdin, Obourg, Vlissingen
CLR2	10 points	Light grey Spiennes
CLR3	12 points	Spiennes
CLR4	15 points	Ère, Esplechin
CLR5	7 points	Esplechin
CLR6	2 points	Spiennes (inclusions)
CLR7	4 points	Spiennes (inclusions)
CLR8	2 points	Light grey Spiennes (inclusions)
CLR9	24 points	Bouvines, Froyennes
CLR10	1 points	Esplechin (inclusion)

To better understand the nature of these clusters, especially the ones containing only few points (probably attributable to inclusions in the flint materials), quantification of the cluster means was performed, yielding the characteristic composition of each cluster. Table 5 lists the concentrations of the cluster means for the elements which showed the greatest variance between the different clusters. The element changing the most proved to be Ca, followed by Sr.

The fit between experiment and simulation was very good in all cases, as demonstrated for one of the larger clusters (CLR4) in Figure 2.

Archaeological Dataset. Because of the unique character of some of the archaeological artefacts, the 18 samples from the archeological data set were neither cut nor polished prior to the experiment, in order to keep these finds intact. The XRF scans were performed on regions of the samples where the interior on the flint samples was visible (as shown in Figure 3 for sample OD2), since it has been proven in the literature that the outer layers, that is the cortex of these types of materials, show great variance in composition.[23] In addition, artefacts with visible surface alterations were avoided in the sampling process. Whenever possible, two different locations on the same sample were scanned, with each time three points being

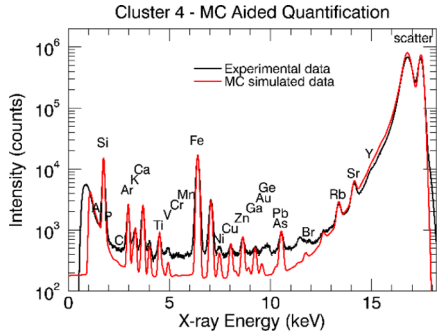

Figure 2. MC aided quantification of CLR4, demonstrating the good fit between the spectra of the experiment and simulation.

measured. Default interspacing of the measurement points was 2 mm, but this could change according to the local circumstances (e.g. size of the sample, free area, surface topography, etc.). The interspacing was always kept at least 0.5 mm to avoid overlap between adjacent measurements. Experimental conditions were identical to the reference sample set.

Data points from the archaeological samples were assigned to 4 of the 10 clusters constructed based on the reference data. These were clusters 1, 4, 5, and 10 as given in Table 4. As can be seen, most points were assigned to clusters containing the bulk of certain types of flint, only 2 points of sample KH2 were assigned to cluster 10, linked with inclusions.

When looking at the samples as a whole instead of individual points, demanding at least half of the points should be assigned to a certain bulk cluster before stating the flint material can be linked to those reference materials, only clusters 1 and 4 remain. As can be seen in Table 6, of the 18 flint samples, 7 do not belong to any of the preconstructed reference clusters according to these criteria. Of the 11 samples that could be assigned, 9 are linked to cluster 4 (materials from Ère or Esplechin) and 2 are linked to cluster 1 (Haubourdin, Obourg, Vlissingen) with some points having deviating compositions not linked to a reference cluster.

DISCUSSION

Clustering Geological Reference Dataset. Finding samples from different locations in the same cluster could have multiple causes depending on the specific cases. For example, cluster 1 groups the Haubourdin, Obourg, and Vlissingen flints together, even though the source locations are far from each other. This can be explained by the similar composition of these flint types, that is very homogenous fine-grained flints with very few/almost no macroscopically visible inclusions. This is further supported by the geochemical quantification of the first cluster which contains the lowest non-silica elemental concentrations (Table 5). Secondly, clusters 4 and 5 group the samples from Ère together with the sample from Esplechin. These samples were collected only 5 km apart and originate from the same geological middle to upper Turonian layers. The same applies for the samples in cluster 9, which consist of samples from Bouvines and samples from Froyennes. These sampling locations are around 14 km apart and also originate from the abovementioned Turonian layers. Then, the question arises why the samples of cluster 4, 5, and 9 are not grouped together since they are from contemporaneous/the same geological layers. This can be explained by comparing the quantified elemental concen-

https://dx.doi.org/10.1021/acs.analchem.0c04583
Anal. Chem. 2021, 93, 3898−3904

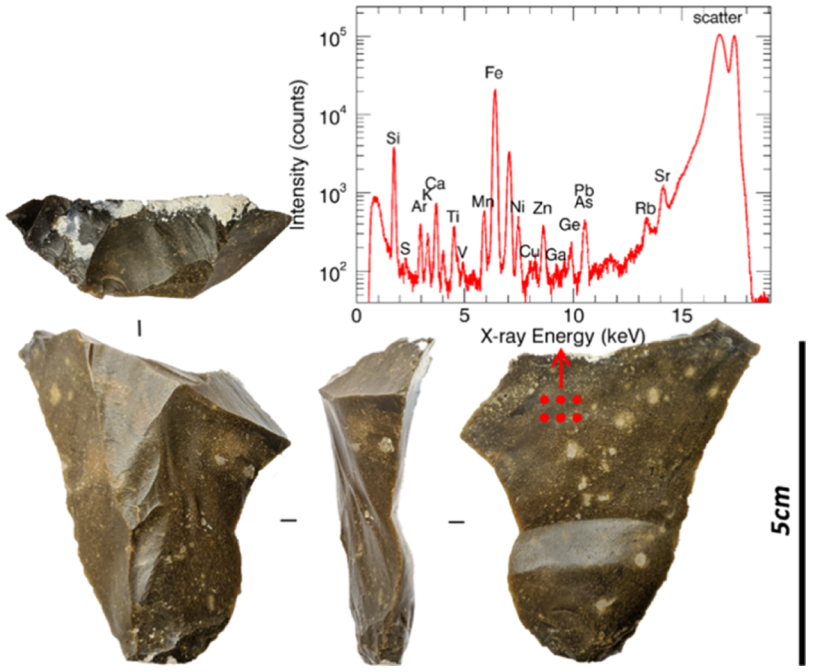

Figure 3. Flint sample (OD 2) with the XRF scanning raster and a point spectrum displayed; 40 kV, 0.8 mA, 3000 s live time.

Table 5. Quantification of the Mean Cluster Compositions for the Elements with the Largest Variance in Their Concentration

	Ca (wt %)	Ti (μg/g)	Fe (μg/g)	Ni (μg/g)	Rb (μg/g)	Sr (μg/g)
CLR1	0.078	40	51	4.5	0.7	2.5
CLR2	2.63	15	80	0.6	0.5	51
CLR3	1.09	50	100	1.2	1.5	47
CLR4	0.068	74	265	1.8	1.6	2.9
CLR5	0.144	74	260	1.8	1.4	9
CLR6	1.05	50	310	1.2	0.5	46
CLR7	2.12	15	125	0.6	0.5	51.5
CLR8	3.69	40	98	4.2	0.7	51
CLR9	0.206	74	180	3.6	1.4	4.4
CLR10	0.075	90	290	1.2	0.5	29.5

trations. The clusters mostly vary in Ca and Sr and Fe and Ni content (Table 2), probably derived from different amounts of carbonate and iron minerals (which are among the major impurities in flint).

The Spiennes flint and its light grey variety were nicely ascribed to two separate clusters, cluster 3 and 2, respectively. Cluster 2 is characterized by a high Ca and Sr content, while cluster 3 has slightly lower Ca and Sr concentrations (but still higher than other major clusters) and higher Ti, Fe, Ni, and Rb concentrations. The Ca and Sr concentrations, which are often positively correlated, point to a composition with higher carbonate content. However, some points of the Spiennes flints were assigned to other clusters: clusters 6, 7, and 8. These can be attributed to inclusions in this very heterogeneous flint type. Given their high Ca and Sr content, they can be linked to carbonate minerals preserved in the remains of carbonate-secreting organisms. Differences occurring between these three clusters lie in the varying Fe and Ni concentrations.

Finally, one point measured on the Esplechin flint was clustered separately (cluster 10). It is characterized by a very high Sr content, but very low Ca content. Also, the Ti and Fe concentrations measured in this point are among the highest of all clusters and could possibly be attributed to the presence of either titanium or iron oxides.

Table 6. Overview of the Archeological Samples with Their Assigned Cluster (If Applicable)

Artefact ID	CLR1[a]	CLR4	not assigned
BA1		×	
BA2		×	
DD1		×	
DD2			×
DD3		×	
DD4			×
DD5			×
DD6	×		
KH1			×
KH2			×
KH3			×
KK1		×	
OD1			×
OD2		×	
OE1		×	
RU1		×	
VA1		×	
VA2	×		

[a]These two samples contained deviating points not assigned to a reference cluster.

The main novelty of this procedure is that trace elements could be analyzed in addition to major elements, in contrast to regular XRF analyses in which the precision of trace elements is not sufficient.[16]

Assignment Archaeological Artefacts. While the majority of the archaeological samples could be assigned to a cluster (11 out of 18), there is still a quite large number that could not be conclusively identified. These findings are in agreement with the results described by Olausson et al. in their work on flint from Northern Europe.[16] However, in contrast to

https://dx.doi.org/10.1021/acs.analchem.0c04583
Anal. Chem. 2021, 93, 3898−3904

the work of these authors, our methodology using monochromatic XRF allows for trace element analysis, which has aided to increase the number of positive identifications.

The fact that only eleven of the 18 archaeological samples were assigned to a certain cluster can have several possible reasons. First, it could be that the source locations of the unassigned artefacts were simply not included in our geological reference dataset, which for the moment only consists of a limited amount of source locations. This could be verified by adding more source locations from the regions already represented in our dataset and/or by expanding our dataset to include samples from the Hesbaye/Limburg area. A second explanation could be that the lateral geochemical variations within a single flint-bearing formation might be greater than expected, making a correct attribution of archaeological artefacts to a specific outcrop more problematic. Perhaps more consideration should be given to the natural variation occurring within these formations. This could be accomplished by sampling more outcrops of the same geological layers. Third, weathering or alteration might have influenced the composition of the archaeological material. While the geological reference samples were measured on unweathered surfaces (inner material), the archaeological samples could have been subjected to post-depositional processes, such as dissolution and leaching (resulting in, e.g., patination), that could have altered the geochemical composition of the outer surface of the artefacts with respect to the inner zone. This phenomenon is well known among archaeologists and should be considered carefully in raw material provenance studies.[12,16,23] Polishing of the archeological artefacts could improve the results but was not implemented as mentioned above because of the unique character of some of the artefacts included. In the future, however, it would be interesting to perform a μXRF-scanning of a control sample of regular debitage products before and after polishing to assess the potential impact of post-depositional weathering on the outer surface of artefacts that at first glance do not appear to be weathered.

When the archaeological artefacts were assigned to a certain cluster, it most of the times corresponded to the expected source location. There are however some exceptions. One archaeological sample, DD6, which was assumed to originate from either Haubourdin or Obourg (based on macroscopic similarities), was correctly assigned to cluster 1. However, VA2, a sample resembling the Spiennes flint, was also assigned to cluster 1 which is not according to our expectations. Six (BA1, KK1, OD2, VA1, DD1, and RU1) samples were successfully assigned to cluster 4, which contains the samples originating from the Tournaisis area. However, two samples, DD3, which was expected to originate from Vlissingen (North Sea basin flint) and BA2, which was expected to be Obourg flint, were assigned to cluster 4, although we expected these samples to be assigned to cluster 1. The sample OE1 was also assigned to cluster 4, however thought to originate from Turonian outcrops in the Mons Basin of which unfortunately no reference sample could be included in the geological reference dataset.

CONCLUSIONS

The refitted microXRF instrument proved a valuable tool for quantitative lab-based XRF experiments. The MC simulation aided quantification procedure based on a large and varied set of reference materials allows standardless quantification of various types of samples, ranging from metal alloys and biological materials to geological or archaeological samples as was demonstrated by the described laboratory XRF-based procedure to analyze and provenance flint materials.

This new provenancing procedure showed promising results, certainly when considering the possibility to further expand the geological reference dataset. The demonstrated methodology, employing a standardized scanning procedure, MC simulation aided quantification and *k*-means clustering could be used in a wide variety of scientific fields and is not limited to the demonstrated test case, which is a notoriously difficult example.

AUTHOR INFORMATION

Corresponding Author

Brecht Laforce − *Department of Analytical Chemistry, X-ray Microspectroscopy and Imaging Research Group (XMI), Ghent University, 9000 Ghent, Belgium;* orcid.org/0000-0002-6561-0948; Email: Brecht.Laforce@UGent.be

Authors

Géraldine Fiers − *Department of Geology, Pore-scale Processes in Geomaterials Research Group (PProGRess)/UGCT, Ghent University, 9000 Ghent, Belgium*

Hans Vandendriessche − *Department of Archaeology, Prehistory Research Group, Ghent University, 9000 Ghent, Belgium*

Philippe Crombé − *Department of Archaeology, Prehistory Research Group, Ghent University, 9000 Ghent, Belgium*

Veerle Cnudde − *Department of Geology, Pore-scale Processes in Geomaterials Research Group (PProGRess)/UGCT, Ghent University, 9000 Ghent, Belgium; Department of Earth Sciences, Environmental Hydrogeology, Utrecht University, 3584 CB Utrecht, The Netherlands*

Laszlo Vincze − *Department of Analytical Chemistry, X-ray Microspectroscopy and Imaging Research Group (XMI), Ghent University, 9000 Ghent, Belgium*

Complete contact information is available at: https://pubs.acs.org/10.1021/acs.analchem.0c04583

Notes

The authors declare no competing financial interest.

ACKNOWLEDGMENTS

This project is funded by the special research fund of Ghent University Special Research Fund (BOF-UGent) (grant number BOF16/IOP/001). B.L. acknowledges financial support by the FWO (grant number 12T2319N).

REFERENCES

(1) Szalóki, I.; Gerényi, A.; Radócz, G.; Lovas, A.; De Samber, B.; Vincze, L. *J. Anal. At. Spectrom.* **2017**, *32*, 334−344.

(2) Tack, P.; Cotte, M.; Bauters, S.; Brun, E.; Banerjee, D.; Bras, W.; Ferrero, C.; Delattre, D.; Mocella, V.; Vincze, L. *Sci. Rep.* **2016**, *6*, 20763.

(3) Radtke, M.; Vincze, L.; Görner, W. *J. Anal. At. Spectrom.* **2010**, *25*, 631−634.

(4) De Samber, B.; Meul, E.; Laforce, B.; De Paepe, B.; Smet, J.; De Bruyne, M.; De Rycke, R.; Bohic, S.; Cloetens, P.; Van Coster, R.; Vandenabeele, P.; Vanden Berghe, T. *PLoS One* **2018**, *13*, No. e0190495.

(5) Carlier, C.; Laforce, B.; Van Malderen, S. J. M.; Gremonprez, F.; Tucoulou, R.; Villanova, J.; De Wever, O.; Vincze, L.; Vanhaecke, F.; Ceelen, W. *J. Pharm. Biomed. Anal.* **2016**, *131*, 256−262.

(6) Terzano, R.; Alfeld, M.; Janssens, K.; Vekemans, B.; Schoonjans, T.; Vincze, L.; Tomasi, N.; Pinton, R.; Cesco, S. *Anal. Bioanal. Chem.* **2013**, *405*, 3341−3350.
(7) Laforce, B.; Masschaele, B.; Boone, M. N.; Schaubroeck, D.; Dierick, M.; Vekemans, B.; Walgraeve, C.; Janssen, C.; Cnudde, V.; Van Hoorebeke, L.; Vincze, L. *Anal. Chem.* **2017**, *89*, 10617−10624.
(8) Schoonjans, T.; Solé, V. A.; Vincze, L.; Sanchez Del Rio, M.; Appel, K.; Ferrero, C. *Spectrochim. Acta, Part B* **2013**, *82*, 36−41.
(9) Garrevoet, J.; Vekemans, B.; Bauters, S.; Demey, A.; Vincze, L. *Anal. Chem.* **2015**, *87*, 6544−6552.
(10) Jack, R. N.; Heizer, R. F. *Contrib. Univ. Calif. Archaeol. Res.* **1968**, *5*, 81−100.
(11) Sieveking, G. D. G.; Bush, P.; Ferguson, J.; Craddock, P. T.; Hughes, M. J.; Cowell, M. R. *Archaeometry* **1972**, *14*, 151−176.
(12) Gauthier, G.; Burke, A. L. *Geoarchaeology* **2011**, *26*, 269−291.
(13) Gauthier, G.; Burke, A. L.; Leclerc, M. *J. Archaeol. Sci.* **2012**, *39*, 2436−2451.
(14) Moreau, L.; Brandl, M.; Filzmoser, P.; Hauzenberger, C.; Goemaere, É.; Jadin, I.; Collet, H.; Hauzeur, A.; Schmitz, R. W. *Geoarchaeology* **2016**, *31*, 229−243.
(15) Olivares, M.; Tarriño, A.; Murelaga, X.; Baceta, J. I.; Castro, K.; Etxebarria, N. *Spectrochim. Acta, Part A* **2009**, *73*, 492−497.
(16) Olausson, D.; Högberg, A.; Hughes, R. E. The Use of Non-Destructive Energy Dispersive X-Ray Fluorescence (EDXRF) Analysis for Sourcing Flint in Northern Europe: Progress to Date and Prospects for the Future. *The Exploitation of Raw Materials in Prehistory: Sourcing, Processing and Distribution*; Pereira, T., Terradas, X., Bicho, N., Eds.; Cambridge Scholars Publishing: Newcastle upon Tyne, 2017; pp 98−112.
(17) Brandl, M.; Hauzenberger, C.; Postl, W.; Modl, D.; Kurta, C.; Trnka, G. *Quartär* **2011**, *58*, 51−65.
(18) Brandl, M.; Hauzenberger, C.; Postl, W.; Martinez, M. M.; Filzmoser, P.; Trnka, G. *Quat. Int.* **2014**, *351*, 146−162.
(19) Moroni, B.; Petrelli, M. *Mediterr. Archaeol. Archaeom.* **2005**, *5*, 49−62.
(20) Neff, H. Laser Ablation ICP-MS in Archaeology. *Handbook of Mass Spectrometry*; Lee, M. S., Ed.; Wiley: New Jersey, 2012; pp 829−843.
(21) Pettitt, P.; Rockman, M.; Chenery, S. *Quat. Int.* **2012**, *272*−*273*, 275−287.
(22) Sánchez de la Torre, M.; Le Bourdonnec, F.-X.; Dubernet, S.; Gratuze, B.; Mangado, X.; Fullola, J. M. *STAR Sci. Technol. Archaeol. Res.* **2017**, *3*, 405−417.
(23) Fernandes, P.; Delvigne, V.; Dubernet, S.; Le Bourdonnec, F.-X.; Morala, A.; Moreau, L.; Piboule, M.; Turq, A.; Raynal, J.-P. *Anthropol. Præhistorica* **2019**, *128/2017*, 263−269.
(24) Parish, R. M.; Swihart, G. H.; Li, Y. S. *Geoarchaeology* **2013**, *28*, 289−307.
(25) Parish, R. M.; Li, Y. S. *Archaeol. Pol.* **2016**, *54*, 115−128.
(26) Crombé, P.; Sergant, J.; Robinson, E.; De Reu, J. *J. Anthropol. Archaeol.* **2011**, *30*, 454−471.
(27) Collin, J.-P. De La Mine à l'habitat: Economie Des Productions Minières Dans Le Bassin de Mons Au Néolithique. De La Fin Du 5e Millénaire à La Fin Du 3e Millènaire Avant Notre Ère. (Unpublished Doctoral Dissertation), Université de Namur et Université Paris 1 Panthéon Sorbonne, 2019.
(28) De Grooth, M. E. T. Distinguishing Upper Cretaceous Flint Types Exploited during the Neolithic in the Region between Maastricht, Tongeren, Liège and Aachen. *Vergangene Zeiten. Liber Amicorum. Gedenkschrift für Jürgen Hoika*; Meurers-Balke, J., Schön, W., Eds.; Deutsche Gesellschaft für Ur- und Frühgeschichte e.V: Bonn, 2011; pp 107−130.
(29) Moreau, L.; Hauzeur, A.; Jadin, I. *Notae Praehistoricae* **2013**, *33*, 105−126.
(30) Fiers, G.; Halbrucker, É.; De Kock, T.; Laforce, B.; Vandendriessche, H.; Messiaen, L.; Vincze, L.; Crombé, P.; Cnudde, V. *Geoarchaeology* **2019**, *34*, 400−412.
(31) Laforce, B.; Vermeulen, B.; Garrevoet, J.; Vekemans, B.; Hoorebeke, L. V.; Janssen, C.; Vincze, L. *Anal. Chem.* **2016**, *88*, 3386−3391.
(32) Jochum, K. P.; Stoll, B.; Herwig, K.; Willbold, M.; Hofmiann, A. W.; Amini, M.; Aarburg, S.; Abouchami, W.; Hellebrand, E.; Mocek, B.; Raczek, I.; Stracke, A.; Alard, O.; Bouman, C.; Becker, S.; Dücking, M.; Brätz, H.; Klemd, R.; De Bruin, D.; Canil, D.; Cornell, D.; De Hoog, C. J.; Dalpé, C.; Danyushevshy, L.; Eisenhauer, A.; Gao, Y.; Snow, J. E.; Groschopf, N.; Günther, D.; Latkoczy, C.; Guillong, M.; Hauri, E. H.; Höfer, H. E.; Lahaye, Y.; Horz, K.; Jacob, D. E.; Kasemann, S. A.; Kent, A. J. R.; Ludwig, T.; Zack, T.; Mason, P. R. D.; Meixner, A.; Rosner, M.; Misawa, K.; Nash, B. P.; Pfänder, J.; Premo, W. R.; Sun, W. D.; Tiepolo, M.; Vannucci, R.; Vennemann, T.; Wayne, D.; Woodhead, J. D. *Geochem., Geophys., Geosyst.* **2006**, *7*, Q02008.
(33) Vekemans, B.; Janssens, K.; Vincze, L.; Adams, F.; Van Espen, P. *X-Ray Spectrom.* **1994**, *23*, 278−285.
(34) Melquiades, F. L.; Santos, S. V.; Lopes, F.; Villanueva, J.; Ticona, J. L.; Appoloni, C. R. *X-Ray Spectrom.* **2020**, *50*, 53.
(35) Wu, X.; Kumar, V.; Ross Quinlan, J.; Ghosh, J.; Yang, Q.; Motoda, H.; McLachlan, G. J.; Ng, A.; Liu, B.; Yu, P. S.; Zhou, Z.-H.; Steinbach, M.; Hand, D. J.; Steinberg, D. *Knowl. Inf. Syst.* **2008**, *14*, 1−37.
(36) Vekemans, B.; Janssens, K.; Vincze, L.; Aerts, A.; Adams, F.; Hertogen, J. *X-Ray Spectrom.* **1997**, *26*, 333−346.
(37) Vekemans, B.; Vincze, L.; Brenker, F. E.; Adams, F. *J. Anal. At. Spectrom.* **2004**, *19*, 1302−1308.

https://dx.doi.org/10.1021/acs.analchem.0c04583
Anal. Chem. 2021, 93, 3898−3904